Inorganica Chimica Acta 585 (2025) 122754

Contents lists available at ScienceDirect

Inorganica Chimica Acta

journal homepage: www.elsevier.com/locate/ica

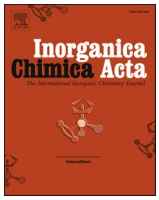

Research paper

Synthesis and structural insights of benzothiazole-appended 2,6-di picolinamide-based Sn(IV) complexes

Tushar S. Basu Baul [a,1,*], Swmkwr Brahma [a], Andrew Duthie [b,2], Sean Parkin [c,*,3]

[a] Centre for Advanced Studies in Chemistry, North-Eastern Hill University, NEHU Permanent Campus, Umshing, Shillong 793 022, India
[b] School of Life & Environmental Science, Deakin University, Pigdons Road, Waurn Ponds, Victoria 3216, Australia
[c] Department of Chemistry, University of Kentucky, 506 Library Drive, 146 Chemistry-Physics Building, Lexington, KY 40506-0055, USA

ARTICLE INFO

Keywords:
Pincer ligand
Benzothiazole scaffold
Diorganotins
Spectroscopy
Crystal structure

ABSTRACT

Four diorganotin complexes of the compositions $[Me_2Sn(L)]\cdot 0.5C_6H_5CH_3$ (**1**), [*n*-$Bu_2Sn(L)$] (**2**), [$Bn_2Sn(L)$] (**3**) and [*n*-$Oct_2Sn(L)$] (**4**) were synthesized by reacting R_2SnO (R = Me, *n*-Bu, Bn or *n*-Oct) with N^2,N^6-bis(benzo[*d*]thiazol-2-yl)pyridine-2,6-dicarboxamide (**H_2L**, where H_2 denotes the two acidic protons) in refluxing toluene. Compounds were characterized by FT-IR (ATR mode), ^{1}H, ^{13}C and ^{119}Sn NMR spectroscopy, as well as high-resolution mass spectrometry. The solid-state structures of compounds **1**–**3,** along with their pro-ligand **H_2L**, were investigated through single-crystal X-ray diffraction studies. In compounds **1**–**3**, the dianionic tridentate pyridine dicarboxamide ligand acts as a κ-N^3 tridentate chelator, coordinating to the equatorial plane, while the coordination sphere of Sn(IV) ion is completed by two axial Sn-R ligands, resulting in a distorted trigonal bipyramidal geometry.

1. Introduction

Benzothiazoles (1,3-benzothiazole) are bicyclic heterocyclic compounds composed of fused benzenic and thiazolic rings, featuring electron-rich heteroatoms nitrogen and sulfur. The unique methine center in the thiazole ring makes benzothiazole one of the most important heterocyclic structures. Benzothiazole derivatives are highly effective with low toxicity, making the benzothiazole scaffold a crucial component in medicinal chemistry [1–5]. In addition to their chemical importance, 2-aminobenzothiazoles have shown a broad spectrum of biological activities, including antiviral [6,7], antimicrobial [7–9], antioxidant [10], anti-inflammatory [11,12], antidepressant [13,14], anti-diabetic [15,16], antitumor [17–19], and antitubercular [20] properties. They have also found applications in organic synthesis and resin production [21,22]. Furthermore, the coordination chemistry of benzothiazole with transition metals enables efficient catalytic processes in organometallic catalysis, with applications spanning organic synthesis to environmental protection [23].

On the other hand, pyridine-2,6-dicarboxamide ligands have attracted considerable attention due to their distinctive characteristics. These include the ability to form a pincer-like structure by combining pyridine and amidic chelating groups, as well as the flexibility to incorporate various substituents and functional groups such as bulky or coordinating atoms onto the amidic nitrogen. This versatility allows for the design of ligands with diverse coordination properties [24,25]. Consequently, these pro-ligand frameworks have been extensively applied in coordinating transition metal ions in catalysis [24–34], sensing [35–45], and other functional and biological fields [46–49]. However, reports on complexation of pyridine-2,6-dicarboxamide ligands with organometallic precursors for the synthesis of organometallic architectures aimed at targeting various challenging organic transformations and applications are limited. To the best of our knowledge, only two reports describe the isolation of diorganotin complexes with N^2,N^6-bis(pyridin-2-yl)pyridine-2,6-dicarboxamide and N^2,N^6-bis(thiazol-2-yl)pyridine-2,6-dicarboxamide [50,51]. The resulting discrete complexes from the former primarily supported catalytic activity in the Baeyer-Villiger oxidation of cyclic ketones to lactones [50], while the latter showed potential as cytotoxic agents against T-47D breast cancer cells [51].

In the light of these considerations, we have integrated the

* Corresponding authors.
E-mail addresses: basubaulchem@gmail.com, basubaul@nehu.ac.in (T.S. Basu Baul).
[1] https://orcid.org/0000-0002-9587-3503.
[2] https://orcid.org/0000-0002-1103-325X.
[3] https://orcid.org/0000-0001-5777-3918.

https://doi.org/10.1016/j.ica.2025.122754
Received 7 April 2025; Received in revised form 5 May 2025; Accepted 7 May 2025
Available online 9 May 2025

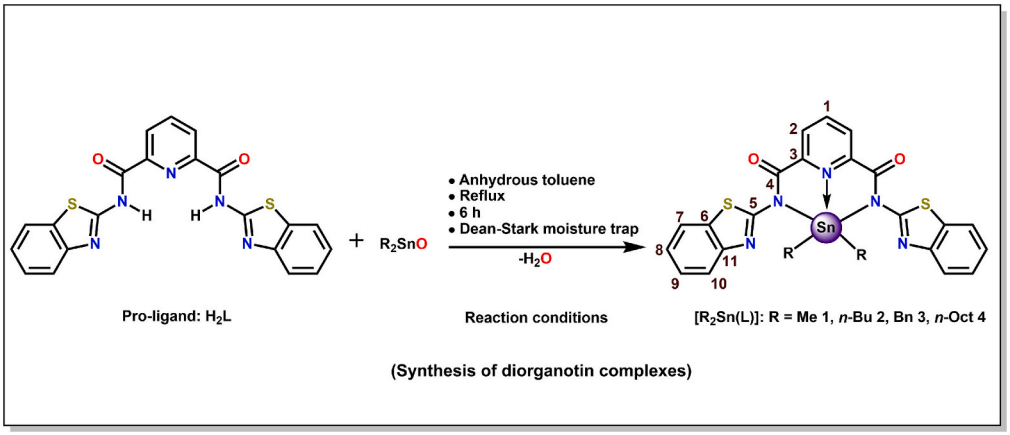

Scheme 1. Reaction sequence for the preparation of pro-ligand N^2,N^6-bis(benzo[*d*]thiazol-2-yl)pyridine-2,6-dicarboxamide (**H_2L**) and diorganotin(IV) compounds (toluene molecule in **1** is not shown), including the alignment of ligand **L** in compounds **1–4** in the solid state.

benzothiazole moiety with pyridine-2,6-dicarboxamide to synthesize N^2,N^6-bis(benzo[*d*]thiazol-2-yl)pyridine-2,6-dicarboxamide (**H_2L**) and explore its reactivity toward organotins (Scheme 1). The pro-ligand **H_2L** features electron-rich heteroatoms and extended π-delocalized systems, in addition to two anionic *N*-amidate donors and a central *N*-pyridyl donor, which could be advantageous for bonding and the generation of supramolecular structures. We present the synthesis of the pro-ligand **H_2L** and its corresponding complexes: $[Me_2Sn(L)]\cdot 0.5C_6H_5CH_3$ (**1**), [*n*-$Bu_2Sn(L)$] (**2**), $[Bn_2Sn(L)]$ (**3**) and [*n*-$Oct_2Sn(L)$] (**4**). All complexes were synthesized and characterized using standard spectroscopic techniques. However, single-crystal X-ray diffraction (SC-XRD) analysis was only possible for compounds **1**–**3** and the pro-ligand **H_2L**.

2. Experimental

2.1. Materials and physical measurements

Thionylchloride, 2,6-pyridinedicarboxylic acid (Spectrochem), dimethyltin oxide (Sigma-Aldrich), di-*n*-butyltin oxide (Merck) and, di-*n*-octyltin oxide and 2-aminobenzothiazole (Fluka) were used as received without further purification. Dibenzyltin dichloride [52] and dibenzyltin oxide [53] were synthesized according to established procedures, and their purity was verified through physical and spectroscopic characterization prior to use. Solvents used in the reactions were of analytical reagent grade and dried according to standard procedures. Toluene and hexane were distilled over benzophenone/sodium, while methanol was distilled over activated magnesium.

Melting points were measured using a Büchi M-560 melting point apparatus and are uncorrected. The Fourier Transform infrared (FT-IR) spectra of the pro-ligand **H_2L** and compounds **1**–**4** were recorded in the range of 400 to 4000 cm^{-1} using a PerkinElmer Spectrum Two spectrometer equipped with UATR accessories, with a resolution of 0.5 cm^{-1}. Solution ^1H (400.13 MHz), ^{13}C (100.62 MHz) and ^{119}Sn (149.15 MHz) nuclear magnetic resonance (NMR) spectra were obtained in $CDCl_3$, unless stated otherwise, on Bruker Avance II 400, AMX 400 or Avance IV 400 spectrometers. Chemical shifts for ^1H, ^{13}C and ^{119}Sn were referenced to Me_4Si (δ 0.00 ppm), $CDCl_3$ (δ 77.00 ppm), and Me_4Sn (δ 0.00 ppm), respectively. Absorption measurements of **H_2L** and compounds **1**–**4** were recorded using an Agilent Technologies Cary 60 spectrophotometer at room temperature in freshly prepared DMSO (spectroscopy grade, Merck). High-resolution mass spectra of **H_2L** and compounds **1**–**4** were acquired on a Waters Xevo G2-XS QTOF mass spectrometer employing electrospray ionization. The fluorescence spectra of **H_2L** and compounds **1**–**4** were measured in freshly prepared DMSO solution using a PTIQM 40 (USA) spectrophotometer. The excitation and emission slits were fixed at 1.25 and 5 nm, respectively, and measurements were conducted in quartz cuvettes with a 10 mm optical path length. Fluorescence quantum yields (ϕ_f) were determined using quinine hemisulfate monohydrate in 0.5 M H_2SO_4 (with $\phi_R = 0.546$) as a standard [54], based on the following equation:

$$\phi_{S=}\ \phi_R \cdot \frac{A_S}{A_R} \cdot \frac{OD_R}{OD_S} \cdot \frac{\eta_S^2}{\eta_R^2}$$

where "A" terms denote the integrated area under the fluorescence curve, "OD" denotes absorbance, "η" the refractive index of the medium, and "ϕ" the fluorescence quantum yield. Subscripts "S" and "R" denote the parameters for the studied sample and reference, respectively. Crystallographic details are given below.

2.2. Synthesis of pro-ligand N^2,N^6-bis(benzo[d]thiazol-2-yl)pyridine-2,6-dicarboxamide, H_2L

The pro-ligand **H_2L** can be synthesized through several methods: (i) by reacting pyridine-2,6-dicarboxylic acid with 2-aminobenzothiazole and triphenylphosphite (M. p.: 288–290 °C) [30]; (ii) by reacting 2-aminobenzothiazole with oxalyl chloride [55]; or (iii) by reacting 2-aminobenzothiazole with pyridine-2,6-dicarbonyl dichloride [31], following the specified reaction conditions and workup procedures. For synthetic convenience, an analogous procedure to the one we previously reported for preparing N^2,N^6-bis(pyridin-2-yl)pyridine-2,6-dicarboxamide and N^2,N^6-bis(thiazol-2-yl)pyridine-2,6-dicarboxamide was used [50,51], where 2-aminopyridine and 2-aminothiazole were replaced with 2-aminobenzothiazole, respectively. Thus, in the present investigation, pyridine-2,6-dicarboxylic acid, thionyl chloride, and 2-aminobenzothiazole are utilized and a detailed procedure is described below.

To a two-necked round-bottomed flask containing a stirring bar, equipped with a condenser and a dropping funnel, 1.0 g (5.983 mmol) **pyridine-2,6-dicarboxylic acid** was transferred and placed in an ice bath. Thionylchloride (15 mL) was then added drop wise under stirring. After the complete addition, the reaction mixture was refluxed with stirring in an oil bath at 80 °C for 5 h. The solution gradually became clear, and the color of the reaction mixture changed to light grey. The reaction mixture was allowed to cool to room temperature, and the excess thionyl chloride was removed under reduced pressure. The solid mass was dissolved in anhydrous toluene (15 mL) and filtered into a 250 mL round-bottom flask containing a stirring bar, keeping the solution hot. To this, a warm toluene solution (15 mL) containing 2-aminobenzothiazole (1.8 g, 11.96 mmol) was added, resulting in the immediate formation of an off-white precipitate. The reaction mixture was again refluxed with stirring at 111 °C for 2 h in an oil bath, by which time the evaluation of HCl had ceased. The precipitate was filtered, rinsed with toluene (2 × 1 mL) and dried. Water was then added to the dried

Table 1
Crystal data, data collection, and refinement statistics for diorganotin compounds **1–3**, and the pro-ligand **H_2L·THF.**

	1	**2**	**3**	**H_2L·THF**
Empirical formula	$C_{53}H_{42}N_{10}O_4S_4Sn_2$	$C_{29}H_{29}N_5O_2S_2Sn$	$C_{35}H_{25}N_5O_2S_2Sn$	$C_{25}H_{21}N_5O_3S_2$
Formula weight	1248.58	662.38	730.41	503.59
Temperature/K	100.0(2)	100.0(2)	100.0(2)	100.0(2)
Crystal system	Monoclinic	Orthorhombic	Monoclinic	Monoclinic
Space group				
	$P2_1/c$	*Pbcn*	$C2/c$	$P2_1/n$
a/Å	14.4749(4)	25.8335(8)	24.4608(4)	16.4044(5)
b/Å	10.7677(2)	14.1829(3)	10.8422(2)	7.7248(6)
c/Å	15.9218(4)	15.0724(4)	25.6841(4)	18.3966(8)
β/°	93.331(1)		97.456(1)	96.665(1)
V/ Å^3	2477.4(1)	5522.4(6)	6754.1(2)	2315.48(15)
Z	2	8	8	4
ρ_{calcd}/cm^3	1.674	1.593	1.437	1.445
μ/mm^{-1}	1.236	1.114	7.483	0.270
F(000)	1252	2688	2944	1048
Reflections collected	45,214	60,767	45,535	41,036
Independent reflections [R_{int}]	5675[0.0336]	6330[0.0539]	6899[0.0345]	5306[0.0557]
Data/restraints/ parameters	5675 / 45 / 364	6330 / 35 / 387	6899 / 0 / 408	5306 / 0 / 322
Goodness-of-fit on F^2	1.095	1.049	1.176	1.052
Final R indexes:				
R_1 [$I \geq 2\sigma$ (I)]	0.0205	0.0224	0.0240	0.0313
wR_2 [all data]	0.0484	0.0564	0.0542	0.0809
($\Delta\rho_{max}/\Delta\rho_{min}$) / e Å^{-3}	0.681/ −0.317	0.755/ −0.328	0.404/ −0.326	0.327/ −0.287
CCDC No.	2,431,628	2,431,629	2,431,630	2,431,631

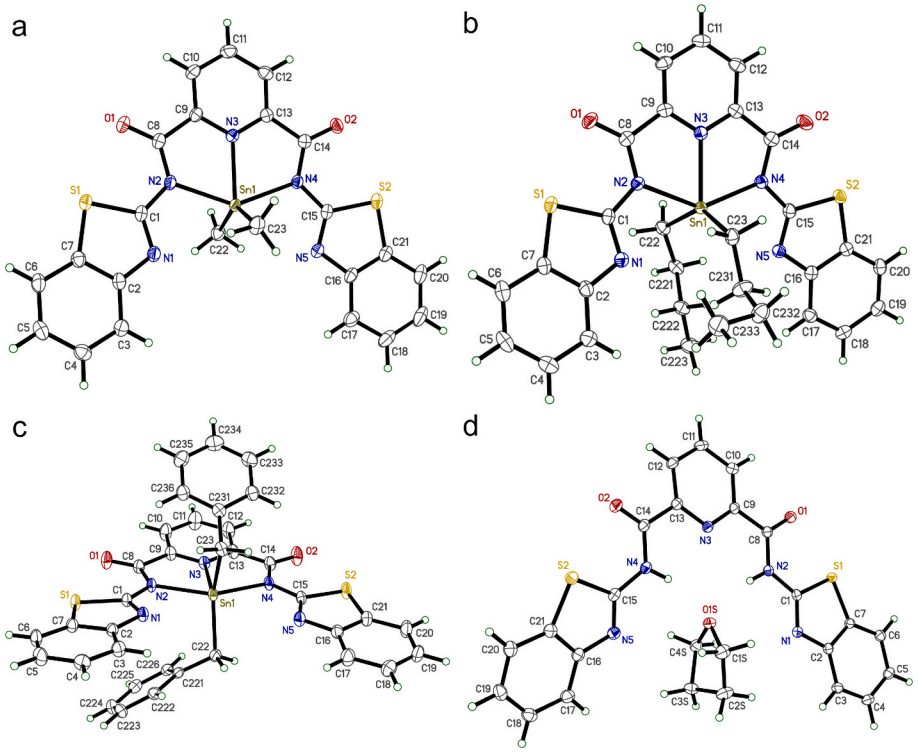

Fig. 1. Displacement ellipsoid plots (50 % probability) for (a) **1**, (b) **2**, (c) **3**, (d) **H_2L·THF** For the sake of clarity, disordered toluene (in **1**) and minor *n*-butyl group disorder (in **2**) are not shown. For ease of comparison, the numbering schemes are consistent across all four structures.

material, which was filtered and transferred into a beaker with the aid of small amount of water. The material was then neutralized with 50 mL of a 10 % $NaHCO_3$ solution and filtered again. Finally, the residue was washed with water until neutral, and then dried. The crude product was crystallized from tetrahydrofuran to yield 1.35 g, (52 %) off-white pro-ligand. M. p.: 290–291 °C. Anal. found: C, 58.66; H, 2.84; N, 16.32 % Anal. calcd. For $C_{21}H_{13}N_5O_2S_2$: C, 58.46; H, 3.04; N, 16.23 %. FT-IR (ATR mode; ν in cm^{-1}): 3237 (w) ν(N—H), 1697 (s) $\nu(C{=}O)_{amide}$, 1596 (w) $\nu(CN)_{py}$, 1537 (vs), 1442 (s), 1303 (m), 1272 (s), 1123 (m), 1066 (m), 1005 (m), 914 (m), 877 (w), 841 (w), 732 (s), 677 (vs), 518 (w). ^{1}H NMR spectrum (DMSO-d_6): δ = 13.65 (s, 2H, H-4), 8.51 (d, 2H, H-2), 8.39 (t, 1H, H-1), 8.10 (d, 2H, H-9), 7.91 (d, 2H, H-8), 7.53 (t, 2H, H-10), 7.40 (t, 2H, H-7) ppm. ^{13}C NMR spectrum (DMSO-d_6): δ = 162.8 (C-5), 158.1 (C-4), 148.6 (C-11), 147.3 (C-3), 140.4 (C-1), 131.7 (C-6), 126.9 (C-9), 126.3 (C-8), 124.0 (C-2), 121.9 (C-7), 120.7 (C-10) ppm. Electronic absorption data (DMSO, λ_{max} [nm]; ε(M^{-1} cm^{-1})): 313; 1662. Emission data (DMSO, λ_{ex} = 313 nm; λ_{em} [nm]; ϕ_f): 480; 0.517. HRMS-ESI$^+$ (m/z, %): found 438.1824 (100), calcd. For [M + Li]$^+$ 438.0671;

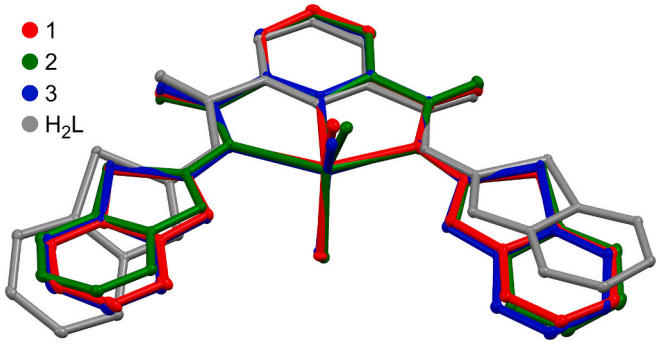

Fig. 2. A least-squares overlay plot of the common cores (*n*-butyl and benzyl groups in **2** and **3** are truncated at the first carbon) of the three tin complexes, showing the similarity of conformations. The pro-ligand **H_2L** is also included to highlight the slight conformational change on binding to Sn.

found 414.0869 (50), calcd. For $[M + H - H_2O]^+$ 414.0483.

2.3. Synthesis of diorganotin(IV) compounds

2.3.1. *[Me_2Sn(L)]·0.5$C_6H_5CH_3$* (**1**)

A 100 mL round-bottom flask was charged with **H_2L** (0.15 g, 0.34 mmol), Me_2SnO (0.057 g, 0.34 mmol), and 50 mL of anhydrous toluene. The flask was equipped with a Dean-Stark trap and a water-cooled condenser, and then heated to reflux. Gradually, the reaction mixture turned pale yellow and became clear. Reflux was maintained for 6 h, after which the mixture was filtered while still hot. The resulting filtrate was evaporated to one-fourth of initial solvent volume using a rotary evaporator and allowed to evaporate slowly at room temperature, yielding pale yellow crystals of the desired product after two days. Yield: 0.12 g (28 %). M.p.: >300 °C. Anal. found: C, 51.28; H, 3.50; N, 11.02. Anal. calcd. For $C_{53}H_{42}N_{10}O_4S_4Sn_2$: C, 50.98; H, 3.39; N, 11.22 %. FT-IR (ATR mode; ν in cm^{-1}): 2926 (w) ν(C—H)$_{aliphatic}$, 1652 (w) ν(C=O)$_{amide}$, 1639 (s), 1595 (m) ν(CN)$_{py}$, 1485 (s), 1439 (s), 1388 (s), 1318 (w), 1272 (w), 1221 (w), 1144 (w), 1032 (w), 985 (m), 930 (m), 751 (sh), 680 (sh), 575 (w). ^{1}H NMR ($CDCl_3$): δ = 8.73 (d, 2H, H-2), 8.54 (t, 1H, H-1), 7.95 (d, 2H, H-9), 7.87 (d, 2H, H-8), 7.48 (t, 2H, H-10), 7.33 (t, 2H, H-7), 7.26 (t, 1H, toluene), 7.16 (t, 2H, toluene), 2.35 (s, 1H, toluene), 1.32 (s, ^2J(^{1}H-$^{117/119}$Sn) 80 Hz, 6H, $SnMe_2$) ppm. ^{13}C NMR ($CDCl_3$): δ = 162.7 (C-5), 160.48 (C-4), 149.0 (C-11), 147.7 (C-3), 145.3 (C-1), 137.8 (C-6), 132.8 (C-9), 129.0 (C-8), 128.2 (C-2), 126.0 (C-7), 125.9 (C-10), 125.2 (toluene), 123.5 (toluene), 121.5 (toluene), 121.1 (toluene), 21.41 (toluene), 5.2 (^1J(^{13}C-$^{117/119}$Sn) 664/695 Hz, $SnMe_2$) ppm. ^{119}Sn NMR ($CDCl_3$): δ = −199.6 ppm. Electronic absorption data (DMSO, λ_{max} [nm]; ε(M^{-1} cm^{-1})): 329; 2940. Emission data (DMSO, λ_{ex} = 329 nm; λ_{em} [nm]; ϕ_f): 405; 0.340. HRMS-ESI$^+$ (*m/z*, %): found 656.0516 (100), calcd. For [M – Me + toluene]$^+$ 656.0237.

2.3.2. *[n-Bu_2Sn(L)]* (**2**)

An analogous method to that used for the preparation of **1** was followed using **H_2L** (0.2 g, 0.46 mmol) and *n*-Bu_2SnO (0.115 g, 0.46 mmol). Pale yellow crystals were obtained from the slow evaporation of the mother liquor for two days. Yield: 0.19 g (63 %). M.p.: 242–243 °C. Anal. found: C, 52.33; H, 4.55; N, 10.88. Anal. calcd. For $C_{29}H_{29}N_5O_2S_2Sn$: C, 52.58; H, 4.41; N, 10.57 %. FT-IR (ATR mode; ν in cm^{-1}): 2924 (w) ν(C—H)$_{aliphatic}$, 1651 (s) ν(C=O)$_{amide}$, 1638 (s), 1597 (w) ν(CN)$_{py}$, 1495 (s), 1443 (s), 1390 (s), 1365 (w), 1320 (w), 1302 (w), 1260 (w), 1160 (s), 1073 (w), 1031 (w), 972 (w), 799 (w), 677 (s), 624 (s), 525 (w). ^{1}H NMR ($CDCl_3$): δ = 8.75 (d, 2H, H-2), 8.57 (t, 1H, H-1), 7.90 (m, 4H, H-8/H-9), 7.49 (t, 2H, H-10), 7.34 (t, 2H, H-7), 2.00 (m, ^2J(^{1}H-$^{117/119}$Sn) 80 Hz, 4H, *n*-Bu-1), 1.54 (m, ^3J(^{1}H-$^{117/119}$Sn) 80 Hz, 4H, *n*-Bu-2), 1.21 (m, 4H, *n*-Bu-3), 0.67 (t, 6H, *n*-Bu-4) ppm. ^{13}C NMR ($CDCl_3$): δ = 162.9 (C-5), 160.9 (C-4), 149.0 (C-11), 148.0 (C-3), 145.1 (C-1), 133.1 (C-6), 126.1 (C-9), 125.9 (C-8), 125.5 (C-2), 121.6 (C-7), 120.9 (C-10), 27.3 (^2J(^{13}C-$^{117/119}$Sn) 42 Hz, *n*-Bu-2), 26.5 (^1J(^{13}C-$^{117/119}$Sn) 600/628 Hz, *n*-Bu-1), 26.2 (^3J(^{13}C-$^{117/119}$Sn) 107 Hz, *n*-Bu-3), 13.5 (*n*-Bu-4) ppm. ^{119}Sn NMR ($CDCl_3$): δ = −227.3 ppm. Electronic absorption data (DMSO, λ_{max} [nm]; ε(M^{-1} cm^{-1})): 330; 2714. Emission data (DMSO, λ_{ex} = 330 nm; λ_{em} [nm]; ϕ_f): 415; 0.222. HRMS-ESI$^+$ (*m/z*, %): found 438.1862 (100), calcd. For [M + Li]$^+$ 438.0671; found 664.0511 (1.83), calcd. For [M + H]$^+$ 664.0863.

2.3.3. *[Bn_2Sn(L)]* (**3**)

An analogous method to that used for the preparation of **1** was followed using **H_2L** (0.2 g, 0.46 mmol) and Bn_2SnO (0.146 g, 0.46 mmol). After filtration and subsequent evaporation, a crude product was obtained. The crude product was dissolved in a minimum amount of benzene, filtered and precipitated with hexane, which was repeated four times. Crystallization from a mixture of anhydrous benzene and hexane (2:1, *v/v*) at room temperature produced pale yellow crystals. Yield: 0.12 g (36 %). M. p.: 152–153 °C. Anal. found: C, 57.38; H, 3.66; N, 9.80

Table 2
Selected bond lengths, angles, and dihedrals in compounds **1–3**, and the pro-ligand **H_2L·THF.**

Atoms	1	2[a]	3	H_2L·THF[b]	JUYWUX[c]
Interatomic distances (Å)					
Sn1-N2	2.2130 (15)	2.2551 (14)	2.1984 (14)	–	–
Sn1-N3	2.2166 (15)	2.2434 (16)	2.2338 (14)	–	–
Sn1-N4	2.2305 (15)	2.2509 (14)	2.2455 (14)	–	–
Sn1-C22	2.1074 (19)	2.1379 (17)	2.1413 (18)	–	–
Sn1-C23	2.1124 (19)	2.128(8)	2.1469 (17)	–	–
N2…O1S[d]	–	–	–	2.9341 (14)	2.975(5)
N4…O1S[d]	–	–	–	2.9106 (15)	2.916(5)
Bond angles involving Sn (°)					
N2-Sn1-N3	71.22(6)	69.98(5)	71.07(5)	–	–
N2-Sn1-N4	142.08(6)	140.75(5)	141.74(5)	–	–
N3-Sn1-N4	70.93(5)	70.79(5)	70.68(5)	–	–
N2-Sn1-C22	97.08(7)	91.11(6)	99.79(6)	–	–
N2-Sn1-C23	97.51(7)	94.1(6)	96.85(6)	–	–
N3-Sn1-C22	110.45(7)	109.86(6)	116.01(6)	–	–
N3-Sn1-C23	112.23(7)	109.9(4)	104.09(6)	–	–
C22-Sn1-C23	137.30(8)	139.2(4)	139.68(7)	–	–
N4-Sn1-C22	98.07(7)	103.21(6)	95.85(6)	–	–
N4-Sn1-C23	94.50(7)	97.9(6)	93.26(6)	–	–
Dihedral angles (°)					
BzT1[e]-*PyC1*[f]	5.18(4)	8.19(6)	12.21(4)	1.47(3)	4.39(18)
BzT2[e]-*PyC2*[f]	2.19(3)	5.85(6)	1.13(3)	20.31(4)	7.28(18)

[a] Only the major disorder component is considered.
[b] Due to the absence of Sn in the pro-ligand, few parameters have analogues in -**H_2L·THF** (or **JUYWUX**).
[c] The numbering scheme in **JUYWUX** was different. The values given here are the nearest equivalents to **H_2L**.
[d] Closest counterpart of Sn—N bonds for **H_2L·THF** are the H-bond donor-acceptor distances.
[e] *BzT*1 is benzothiazole fragment N1,S1,C1-C7; BzT2 is N5,S2,C15-C21.
[f] *PyC*1 is pyridine-2-carboxamide fragment O1,N2,N3,C8-C13; PyC2 is O2,N3, N4,C9-C14.

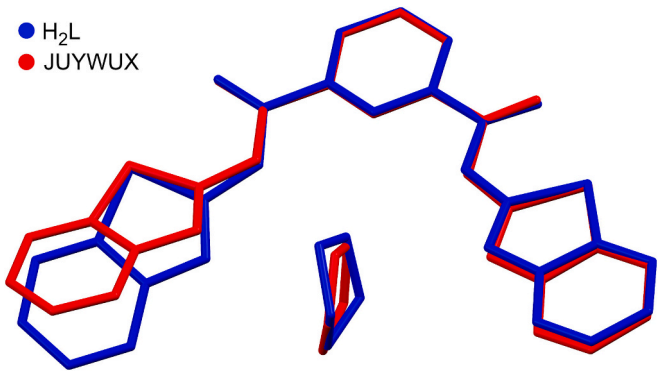

Fig. 3. A least-squares overlay plot of the pro-ligand **H_2L** with bound THF (in blue) and a polymorphic structure (JUYWUX) found in the CSD (Cambridge Structural Database).

Anal. calcd. For $C_{35}H_{25}N_5O_2S_2Sn$: C, 57.55; H, 3.45; N, 9.59 %. FT-IR (ATR mode; ν in cm^{-1}): 2924 (w) ν(C—H)$_{aliphatic}$, 1651 (s) ν(C=O)$_{amide}$, 1639 (s), 1594 (m) ν(CN)$_{py}$, 1485 (s), 1440 (s), 1375 (s), 1275 (m), 1251 (w), 1228 (w), 1081 (w), 1028 (m), 984 (m), 933 (w), 763 (sh), 684 (w), 549 (w). ^{1}H NMR ($CDCl_3$): δ = 8.20 (d, 2H, H-2), 8.19 (t, 1H, H-1), 8.07 (d, 2H, H-9), 7.96 (d, 2H, H-8), 7.57 (t, 2H, H-10), 7.41 (t, 2H, H-7), 6.68 (m, 6H, Bz-4/Bz-5), 6.52 (d, 4H, Bz-3), 3.53 (s, ^2J (^{1}H-$^{117/119}$Sn) 84 Hz, 4H, Bz-1) ppm. ^{13}C NMR ($CDCl_3$): δ = 163.0 (C-5), 160.6 (C-4), 149.0 (C -11), 146.9 (C-3), 144.3 (C-1), 136.6 (Bz-2), 132.9 (C-6), 127.9 (Bz-4), 127.2 (Bz-3), 126.1 (Bz-5), 125.2 (C-9), 125.0 (C-8), 123.7 (C-2), 121.7 (C-7), 121.1 (C-10), 34.2 ($SnBz_2$) ppm. ^{119}Sn NMR ($CDCl_3$): δ = −294.1 ppm. Electronic absorption data (DMSO, λ_{max} [nm]; ε(M^{-1} cm^{-1})): 330; 1941. Emission data (DMSO, λ_{ex} = 330 nm; λ_{em} [nm]; ϕ_f): 415; 0.407. HRMS-ESI$^+$ (*m/z*, %): found 732.0638 (57), calcd. For $[M + H]^+$ 732.0550.

2.3.4. *[n-Oct$_2$Sn(L)] (**4**)*

An analogous method to that used for the preparation of **1** was

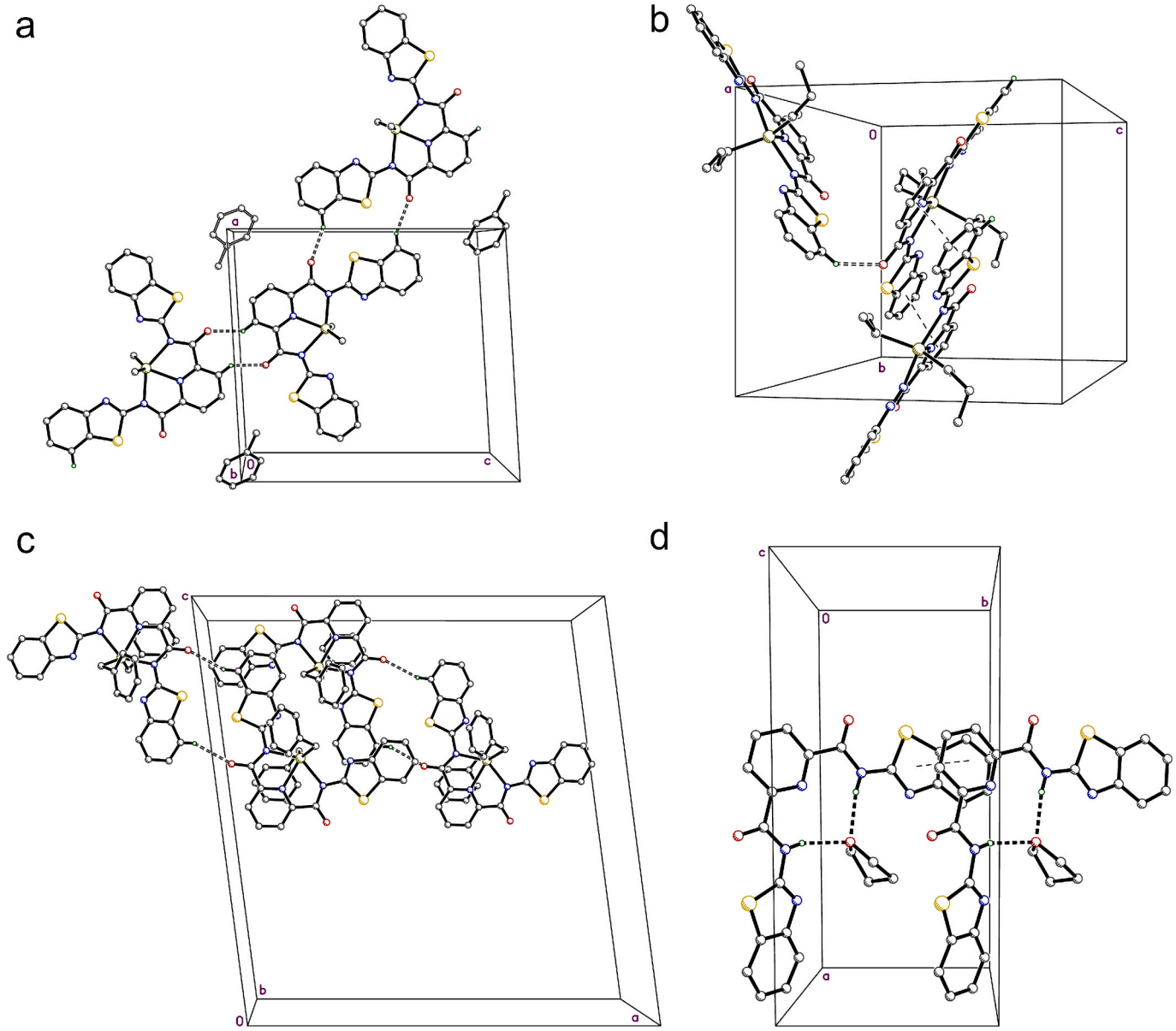

Fig. 4. Partial packing plots for (a) **1**, (b) **2**, (c) **3**, (d) **H_2L** showing the most structurally important intermolecular interactions. Unconventional weak C-H…O hydrogen bonds in **1**, **2**, **3** are shown as open dashed lines, π…π overlapped rings are indicated by single-dashed lines in **2** and **H_2L**, and conventional N-H…O$_{THF}$ hydrogen bonds between the pro-ligand and THF solvent are shown as thick dashed lines.

followed using **H_2L** (0.2 g, 0.46 mmol) and *n*-Oct_2SnO (0.167 g, 0.46 mmol). After filtration and subsequent evaporation, a crude product was obtained. The crude product was dissolved in a minimum amount of benzene, filtered and precipitated with hexane; this process was repeated several times. Crystallization from hexane at room temperature produced pale yellow microcrystalline material. Yield: 0.21 g (60 %) M. p.: 140–141 °C. Anal. found: C, 57.55; H, 6.16; N, 8.84. Anal. calcd. For $C_{37}H_{45}N_5O_2S_2Sn$: C, 57.37; H, 5.86; N, 9.04 %. FT-IR (ATR mode; ν in cm^{-1}): 2922 (w) ν(C—H)$_{aliphatic}$, 1651 (w) ν(C=O)$_{amide}$, 1640 (*s*), 1600 (m) ν(CN)$_{py}$, 1490 (s), 1438 (s), 1370 (s), 1269 (m), 1226 (w), 1147 (w), 1015 (w), 984 (m), 929 (m), 796 (w), 751 (w), 683 (w). ^{1}H NMR ($CDCl_3$): δ = 8.75 (d, 2H, H-2), 8.57 (t, 1H, H-1), 7.89 (m, 4H, H-8/H-9), 7.49 (t, 2H, H-10), 7.34 (t, 2H, H-7), 2.00 (m, ^2J(^{1}H-$^{117/119}$Sn) 76 Hz, 4H, *n*-Oct-1), 1.57 (m, ^3J(^{1}H-$^{117/119}$Sn) 99 Hz, 4H, *n*-Oct-2), 1.12 (m, 12H, *n*-Oct-3/*n*-Oct-6/ *n*-Oct-7), 1.02 (m, 8H, *n*-Oct-4/*n*-Oct-5), 0.77 (t, 6H, *n*-Oct-8) ppm. ^{13}C NMR ($CDCl_3$): δ = 162.9 (C-5), 160.0 (C-4), 149.0 (C-11), 148.0 (C-3), 146.0 (C-1), 130.0 (C-6), 126.0 (C-9), 125.9 (C-8), 123.5 (C-2), 121.6 (C-7), 120.9 (C-10), 33.0 (^3J(^{13}C-$^{117/119}$Sn) 103 Hz, *n*-Oct-3), 31.6 (*n*-Oct-6), 29.0 (*n*-Oct-5), 28.8 (*n*-Oct-4), 26.7 (*n*-Oct-1), 25.1 (^2J(^{13}C-$^{117/119}$Sn) 41 Hz, *n*-Oct-2), 22.5 (*n*-Oct-7), 14.0 (*n*-Oct-8) ppm. ^{119}Sn NMR ($CDCl_3$): δ = −227.3 ppm. Electronic absorption data (DMSO, λ_{max} [nm]; ε (M^{-1} cm^{-1})): 330; 2014. Emission data (DMSO, λ_{ex} = 330 nm; λ_{em} [nm]; ϕ_f): 415; 0.278. HRMS-ESI$^+$ (*m/z*, %): found 776.2305 (0.39), calcd. For $[M + H]^+$ 776.2115.

2.4. X-ray crystallography

Single crystals suitable for X-ray structure determination were grown from various solvent combinations: **H_2L** from THF, **1** and **2** from toluene, and **3** from benzene/hexane (2:1, *v*/v). In addition, crystals of **4** were obtained from a solution in hexane, but proved to be unsuitable for X-ray analysis. Suitable specimens of **H_2L**, **1**, and **2** were individually mounted on nylon loops, whereas the crystal of **3** was mounted on a fine glass fibre embedded in a copper-mounting pin [56]. Diffraction data were collected at 100.0(2) K using a dual-microsource Bruker D8 Venture diffractometer with Mo*Kα* radiation (λ = 0.71073 Å) for **H_2L**, **1**, and **2**, and CuKα radiation (λ = 1.54178 Å) for **3**. Data collection and reduction [57] absorption correction [58,59], structure solution [60], and refinement [61] were carried out using common programs and procedures. Crystals of **H_2L** were THF solvates; **1** contained disordered toluene; **2** was solvent free; and **3** had poorly defined solvent, handled using the *SQUEEZE* routine in *PLATON* [62].

3. Results and discussion

3.1. Design aspects, synthesis and spectroscopic characterization

Although the pro-ligand *N*^{2},*N*^{6}-bis(benzo[*d*]thiazol-2-yl)pyridine-2,6-dicarboxamide (**H_2L**) can be synthesized using methods described in the literature [30,31,55], for synthetic convenience, in the present investigation a two-stage process was followed. Initially, pyridine-2,6-dicarboxylic acid was treated with thionyl chloride to produce pyridine-2,6-dicarbonyl dichloride. This intermediate was then reacted with two equivalents of 2-aminobenzothiazol in anhydrous toluene, yielding the desired pro-ligand. The diorganotin compounds **1**–**4** were prepared by refluxing equimolar quantities of **H_2L** with the respective R_2SnO compounds (where R = Me, *n*-Bu, Bn, or *n*-Oct) in toluene. During the reaction, water was removed via azeotropic distillation. The pale yellow compounds of compositions $[Me_2Sn(L)]\cdot 0.5C_6H_5CH_3$ (**1**), [*n*-$Bu_2Sn(L)$] (**2**), [$Bn_2Sn(L)$] (**3**) and [*n*-$Oct_2Sn(L)$] (**4**) were obtained upon crystallization with the appropriate solvent(s) (Scheme 1).

These compounds have shown remarkable stability in both their solid state and in solution, as confirmed by various analytical techniques including X-ray diffraction, ^{119}Sn NMR and electronic spectroscopy. Pro-ligand **H_2L** displayed a prominent absorption peak at ca. λ_{max} 313 nm in DMSO, which is characteristic of an n → π* transition. In compounds **1**–**4**, this peak shifts to a longer wavelength (bathochromic shifts) and settles at 330 nm (ESI Fig. S1) [30,31], suggesting that these compounds retain similar five-coordinate geometries in solution. This was subsequently confirmed from the results of ^{119}Sn NMR (vide infra). Pro-ligand **H_2L** exhibited a sharp and intense emission spectral band at 480 nm, while its complexes **1**–**4** exhibited spectral bands in a narrow range of 405–415 nm in DMSO (ESI Fig. S2). The fluorescent quantum yield for the **H_2L** was found to be 0.517, while lower yields were found for compounds **1**–**4**, i.e. 0.340, 0.222, 0.407, and 0.278, respectively. The FT-IR (ATR mode) absorptions data detailed in the Experimental section (ESI Figs. S3-S7), show that the ν(NH) band present at 3237 cm^{-1} in **H_2L** is missing in compounds **1**–**4**. This suggests that the deprotonated $N_{amidate}$ atoms are involved in bonding in a tripodal fashion [51,63]. Additionally, the ν(C=O)$_{amide}$ peak shifts from 1697 cm^{-1} in **H_2L** to 1651 cm^{-1} in compounds **1**–**4**, providing further evidence for bonding interaction. The characterization of both the pro-ligand **H_2L** and compounds **1**–**4** in solution were performed using ^{1}H and ^{13}C NMR spectra (ESI Figs. S8-S17), while the solution behavior of compounds **1**–**4** was assessed through ^{119}Sn NMR (ESI Figs. S18-S21). In general, the ^{1}H and ^{13}C NMR spectra of **H_2L** and compounds **1**–**4** exhibited a single set of signals corresponding to the expected ^{1}H and ^{13}C resonance peaks in the aromatic and aliphatic regions (for tin compounds). This suggests that, in solution, both the ligand arms and the Sn-R groups are magnetically equivalent. The ^{1}H NMR spectrum of **H_2L** shows a singlet at δ 13.65 ppm, corresponding to the N—H group. This signal is absent in compounds **1**–**4**, likely due to the doubly deprotonated state of the ligand and coordination of the amidate nitrogen atoms to the tin atom [50,51]. Additionally, the ^{1}H and ^{13}C NMR spectra of **H_2L** and its compounds **1**–**4** displayed various signals corresponding to the central *N*-pyridyl donor, the pendant heterocyclic benzothiozoles rings, and the Sn-R groups, which are not discussed further. The dialkyltin compounds **1**, **2**, and **4** exhibit a sharp singlet in the range of δ −199.6 to −227.3 ppm, while dibenzyltin compound **3** shows a signal at δ −294.1 ppm (ESI Figs. S18-S21). The δ(^{119}Sn) values align well with the expected δ(^{119}Sn) values for corresponding diorganotin compounds, which fall within the anticipated range for five-coordinate geometries with a cognate pincer ligand featuring a κ-*N*^{3} tridentate chelator [50,51]. The mass-to-charge ratios of the ions for **H_2L** and diorganotin compounds **1**–**4** were determined in acetonitrile solution using high-resolution mass spectrometry (ESI Figs. S22-S26). The $[M + Li]^+$ ion, with a peak intensity of 100 %, was most notably observed for the pro-ligand **H_2L** and compound **2**. Additionally, diorganotin compounds **2**–**4** displayed $[M + H]^+$ ions, as well as other peaks represented fragments of the parent ions due to the loss of various groups, though these fragments could not be analyzed further.

3.2. Description of the solid-state structures

Crystal data, data collection and refinement statistics for **1**–**3**, and the pro-ligand **H_2L·THF** are given in Table 1. Ellipsoid plots showing the molecular structures of compounds **1**–**3**, and **H_2L·THF** are presented in Fig. 1, additional packing plots are provided in ESI Figs. S27-S38. There are no unusual bond lengths or angles in any of the structures (for full tables, refer to the ESI Tables S1-S4).

In structures **1**, **2**, and **3**, the Sn atoms are five-coordinate with distorted trigonal bipyramidal geometries. In the equatorial plane, Sn1 bonds to the pyridine N3 and carbons C22/C23 of the methyl (**1**), *n*-butyl (**2**), or benzyl (**3**) ligands, with axial bonds to N2 and N4 of the chelating **L**-ligand. The degree of distortion is similar in each case and is forced by the substantial deviation of bonds N2-Sn1-N4 (142.08(6)°, 140.75(5)°, 141.74(5)° in **1**, **2**, **3**, respectively) from the ideal axial angle of 180°. This is shown in a qualitative way in Fig. 2 and quantified in Table 2. The geometry about the Sn atom in each of **1**, **2**, **3** is in fact substantially similar to those in a series of related Sn-thiazole compounds [51], for which the N2-Sn1-N4 axial bond angles ranged between 142.19° and 143.66°. Equatorial distortions from the ideal 120° also follow similar trends to those in the Sn-thiazole analogues. Due to the constraining

nature of the chelating ligand, these angles range from 104.09(6)° for N3-Sn1-C23 in **3** to 116.01(6)° for N3-Sn1-C22 in **3** (cf. 107.92(5)° to 118.35(9)° in the series of Sn-thiazoles) and 137.20(8)°, 139.2(4)°, and 138.68(7)° for C22-Sn1-C23 in **1**, **2**, **3** respectively (cf. 130.449(12)° to 137.47(6)° in the Sn-thiazoles). The crystal structure of **1** includes a statistically (50:50) disordered toluene solvent molecule situated on an inversion centre, but the Sn-complex itself is not disordered. Structure **2** is solvent free but includes two-component disorder of one of its pendant butyl groups (refined occupancy factors are ~56 % and ~44 %). In **3**, the Sn-complex is fully ordered, but the crystal structure incorporates solvent accessible regions that contained disordered solvent. These crystals grew from a benzene/hexane mixed solvent system, for which no satisfactory model could be made, so the solvent contributions were subtracted using *SQUEEZE* in *Platon* [62].

The pro-ligand structure is not disordered but includes a THF solvent molecule bound to the **H_2L** pro-ligand by a pair of conventional hydrogen bonds, N2-H2N…O1S and N4-H4N…O1S, for which the donor…acceptor distances are 2.9341(14) Å and 2.9106(15) Å, respectively. A polymorph of the **H_2L·THF** solvate crystal structure exists in the CSD, refcode JUYWUX [64]. These two structures have different settings of the same type of space group ($P2_1/n$ in this work vs. $P2_1/c$ in JUYWUX), but the structures are distinct (i.e., they cannot be transformed onto one another by any valid crystallographic operation). In the room-temperature JUYWUX structure, the THF is almost certainly disordered, though it was not modelled as such; it is bound in a similar way by two N-H…O_{THF} hydrogen bonds, but the conformation of the **H_2L** moiety is different, as shown in an overlay plot (Fig. 3) and quantified in the dihedral angles between the benzothiazole and pyridine-2-carboxamide fragments (Table 2).

In the crystal packing of **1**, **2**, and **3** there are no conventional hydrogen bonds, but there are a number of weak C-H…O hydrogen bonds and other types of intermolecular interactions (Fig. 4). In **1**, two such weak interactions are flagged as potential hydrogen bonds by *SHELXL* [61], namely H-bonds C6-H6…O1(-x + 2,-y + 1,-z + 1) and C12-H12…O2(-x + 1,-y + 1,-z), with long donor-acceptor distances ($d_{D\text{-}A}$) of 3.360(2) Å and 3.213(2) Å. Each occurs as inversion-related pairs, leading to flattened chains that propagate parallel to [101], as shown in Fig. 4a. No π…π-stacking is evident, but there are C—H..π close contacts (as flagged by *Mercury* [65]) involving the disordered toluene but these are unlikely to be structurally important. In **2**, a long H-bond like contact C20-H20…O1(-x + 3/2,-y + 1/2,z + 1/2), $d_{D\text{-}A}$ = 3.336(2)Å joins 2_1 screw-related molecules, while glide-related (-x + 3/2,y + 1/2,z) molecules exhibit weak π…π interactions (Fig. 4b) that asymmetrically overlap pyridine and benzene rings giving centroid-centroid distances of 3.786 Å and 3.896 Å, but the pairs of stacked rings are not quite parallel (dihedrals = 12.14(9)° and 6.22(10)°). For structure **3**, weak interactions of the form C6-H6…O1(-x,y,-z + 3/2), $d_{D\text{-}A}$ = 3.380(2) Å, link pairs of molecules into loose dimers about crystallographic 2-fold axes parallel to the *b*-axis (Fig. 4c). There are no other noteworthy intermolecular contacts. Lastly, in the structure of **H_2L**, other than the N-H…O_{THF} hydrogen bonds mentioned above, the pyridine and thiazole (S1, N1,C1,C2,C7) rings of adjacent (x,1 + y,z) molecules π-stack with a centroid-to-centroid distance of 3.518 Å to generate chains that propagate parallel to the *b*-axis (Fig. 4d). Similar contacts occur in the polymorph, JUYWUX.

4. Conclusions

This article discusses a comprehensive study involving the design and synthesis of a pioneering pyridine-2,6-dicarboxamide-based pincer-type pro-ligand, specifically benzothiazole-appended 2,6-di picolinamide, and its diorganotin compounds. A series of stable, neutral diorganotin compounds were efficiently synthesized and characterized through elemental and spectroscopic analyses, as well as X-ray crystallography (with the exception of compound **4**). High-resolution mass spectrometry (HRMS) confirmed the stability of all the five-coordinate Sn(IV) compounds in acetonitrile solution. The structural architectures were carefully examined in both solution and solid state. X-ray diffraction analysis revealed that in diorganotin compounds **1**–**3**, the dianionic tridentate ligand forms κ-N^3 chelates, giving a distorted trigonal bipyramidal geometry around the tin atom. Tin NMR data shows that the five-coordinate structures in the solid state are preserved in deuterated chloroform solution. Diffraction results indicate that a pincer cavity, featuring two pendant benzothiazole rings, comfortably accommodates various R_2Sn(IV) ions. This comprehensive research initiative has the potential to transcend the confines of our laboratory, making a pivotal step not only toward biological significance but also toward structural and catalytic relevance.

CRediT authorship contribution statement

T.S.B.B.: Conceptualization, investigation, project administration, resources, supervision, writing original draft, review and editing; S.B.: Experiments, Data curation, investigation, methodology, software validation; A.D: Data curation, formal analysis, review; S.P.: Resources, Software validation, data curation, review, editing.

Declaration of competing interest

The authors declare that they have no known competing financial interests or personal relationships that could have appeared to influence the work reported in this paper.

Acknowledgements

SB thanks University Grants Commission, New Delhi for the award of non-NET fellowships. Authors (TSBB and SB) thank SAIF-NEHU, Shillong for providing NMR measurements and the DST-FIST program (No. SR/FST/CS-II/2019/99(C)), Government of India, for providing the HRMS instrument to the Department of Chemistry, NEHU, Shillong. Deakin University's Advanced Characterization Facility is acknowledged for use of the NMR instrumentation. SP thanks the US NSF MRI program (grant CHE-1625732).

Appendix A. Supplementary data

Supplementary data to this article can be found online at https://doi.org/10.1016/j.ica.2025.122754.

Data availability

Data Provided in SI

References

[1] R.S. Keri, M.R. Patil, S.A. Patil, S. Budagumpi, A comprehensive review in current developments of benzothiazole-based molecules in medicinal chemistry, Eur. J. Med. Chem. 89 (2015) 207–251.
[2] A. Rouf, C. Tanyeli, Bioactive thiazole and benzothiazole derivatives, Eur. J. Med. Chem. 97 (2015) 911–927.
[3] S. Agarwal, D. Gandhi, P. Kalal, Benzothiazole: a versatile and multitargeted pharmacophore in the field of medicinal chemistry, Lett. Org. Chem. 14 (2017) 729–742.
[4] Y.I. Asiri, A. Alsayari, A.B. Muhsinah, Y.N. Mabkhot, M.Z. Hassan, Benzothiazoles as potential antiviral agents, J. Pharm. Pharmacol. 72 (2020) 1459–1480.
[5] X. Liu, Z.B. Dong, A review on domino condensation/cyclization reactions for the synthesis of 2-substituted 1,3-benzothiazole derivatives, Eur. J. Org. Chem. 2020 (2020) 408–419.
[6] F.M. Shaikh, N.B. Patel, G. Sanna, B. Busonera, P.L. Colla, D.P. Rajani, Synthesis of some new 2-amino-6-thiocyanato benzothiazole derivatives bearing 2,4-thiazolidinediones and screening of their in vitro antimicrobial, antitubercular and antiviral activities, Med. Chem. Res. 24 (2015) 3129–3142.
[7] M.B. Elamin, A.A.E.S.A. Elaziz, E.M. Abdallah, Benzothiazole moieties and their derivatives as antimicrobial and antiviral agents: a mini-review, Int. J. Res. Pharm. Sci. 11 (2020) 3309–3315.

[8] I. Defrenza, A. Catalano, A. Carocci, A. Carrieri, M. Muraglia, A. Rosato, F. Corbo, C. Franchini, 1,3-Benzothiazoles as antimicrobial agents, J. Heterocyclic Chem. 52 (2015) 1705–1712.

[9] E. Chugunova, C. Boga, I. Sazykin, S. Cino, G. Micheletti, A. Mazzanti, M. Sazykina, A. Burilov, L. Khmelevtsova, N. Kostina, Synthesis and antimicrobial activity of novel structural hybrids of benzofuroxan and benzothiazole derivatives, Eur. J. Med. Chem. 93 (2015) 349–359.

[10] R. Bala, P. Kumari, S. Sood, V. Kumar, N. Singh, K. Singh, Phthaloyl dichloride-DMF mediated synthesis of benzothiazole-based 4-formylpyrazole derivatives: studies on their antimicrobial and antioxidant activities, J. Heterocyclic Chem. 55 (2018) 2507–2516.

[11] S. Tariq, O. Alam, M. Amir, Synthesis, p38α MAP kinase inhibition, anti-inflammatory activity, and molecular docking studies of 1,2,4-triazole-based benzothiazole-2-amines, Arch. Pharm. Chem. Life Sci. 351 (2018) e1700304.

[12] S. Tariq, P. Kamboj, O. Alam, M. Amir, 1,2,4-Triazole-based benzothiazole/benzoxazole derivatives: design, synthesis, p38α MAP kinase inhibition, anti-inflammatory activity and molecular docking studies, Bioorg. Chem. 81 (2018) 630–641.

[13] Ü.D. Özkay, C. Kaya, U.A. Çevik, Ö.D. Can, Synthesis and antidepressant activity profile of some novel benzothiazole derivatives, Molecules 22 (2017) 1490, https://doi.org/10.3390/molecules22091490.

[14] Ü.D. Özkay, Ö.D. Can, B.N. Saglik, U.A. Çevik, S. Levent, Y. Özkay, S. Ilgın, Ö. Atlı, Design, synthesis, and AChE inhibitory activity of new benzothiazole-piperazines, Bioorg. Med. Chem. Lett. 26 (2016) 5387–5394.

[15] G. Sadhasivam, K. Kulanthai, Synthesis, characterization, and evaluation of anti-inflammatory and anti-diabetic activity of new benzothiazole derivatives, J. Chem. Pharm. Res. 7 (2015) 425–431.

[16] K. Harrouche, J.-F. Renard, N. Bouider, P. Tullio, E. Goffin, P. Lebrun, G. Faury, B. Pirotte, S. Khelili, Synthesis, characterization and biological evaluation of benzothiazoles and tetrahydrobenzothiazoles bearing urea or thiourea moieties as vasorelaxants and inhibitors of the insulin releasing process, Eur. J. Med. Chem. 115 (2016) 352–360.

[17] T.L. Dadmal, K. Appalanaidu, R.M. Kumbhare, T. Mondal, M.J. Ramaiah, M. P. Bhadra, Synthesis and biological evaluation of triazole and isoxazole-tagged benzothiazole/benzoxazole derivatives as potent cytotoxic agents, New J. Chem. 42 (2018) 15546–15551.

[18] F. Sultana, M.A. Saifi, R. Syed, G.S. Mani, S.P. Shaik, E.G. Osas, C. Godugu, S. Shahjahanb, A. Kamal, Synthesis of 2-anilinopyridyl linked benzothiazole hydrazones as apoptosis inducing cytotoxic agents, New J. Chem. 43 (2019) 7150–7161.

[19] N. Pathak, E. Rathi, N. Kumar, S.G. Kini, C.M. Rao, A review on anticancer potentials of benzothiazole derivatives, Mini-Rev. Med. Chem. 20 (2020) 12–23.

[20] R. Yadav, D. Meena, K. Singh, R. Tyagi, Y. Yadav, R. Sagar, Recent advances in the synthesis of new benzothiazole based anti-tubercular compounds, RSC Adv. 13 (2023) 21890–21925.

[21] R. Jian, P. Wang, W. Duan, J. Wang, X. Zheng, J. Weng, Synthesis of a novel P/N/S-containing flame retardant and its application in epoxy resin: thermal property, flame retardance, and pyrolysis behavior, J. Ind. Eng. Chem. Res. 55 (2016) 11520–11527.

[22] X. Gao, J. Liu, X. Zuo, X. Feng, Y. Gao, Recent advances in synthesis of benzothiazole compounds related to green chemistry, Molecules 25 (2020) 1675, https://doi.org/10.3390/molecules25071675.

[23] T.M.V.D. Pinho, M. Pineiro e Melo, Heterocycles: synthesis, catalysis, sustainability, and characterization, in: T.M.V.D. Pinho e Melo, M. Pineiro (Eds.), Wiley-VCH GmbH, Weinhem, Germany, 2022, https://doi.org/10.1002/9783527832002.

[24] P. Kumar, R. Gupta, The wonderful world of pyridine-2,6-dicarboxamide based scaffolds, Dalton Trans. 45 (2016) 18769–18783.

[25] S. Pachisia, R. Gupta, Architectural and catalytic aspects of designer materials built using metalloligands of pyridine-2,6-dicarboxamide based ligands, Dalton Trans. 49 (2020) 14731–14748.

[26] a T.C. Harrop, P.K. Mascharak, Fe(III) and co(III) centers with carboxamido nitrogen and modified sulfur coordination: lessons learned from nitrile hydratase, Acc. Chem. Res. 37 (2004) 253–260;
b A. Rajput, R. Mukherjee, Coordination chemistry with pyridine/pyrazine amide ligands. Some noteworthy results, Coord. Chem. Rev. 257 (2013) 350–368;
c D.S. Marlin, P.K. Mascharak, Coordination of carboxamido nitrogen to tervalent iron: insight into a new chapter of iron chemistry, Chem. Soc. Rev. 29 (2000) 69–74.

[27] M.J. Rose, P.K. Mascharak, Photoactive ruthenium nitrosyls: effects of light and potential application as NO donors, Coord. Chem. Rev. 252 (2008) 2093–2114.

[28] F.A. Chavez, P.K. Mascharak, Co(III)-alkylperoxo complexes: syntheses, structure-reactivity correlations, and use in the oxidation of hydrocarbons, Acc. Chem. Res. 33 (2000) 539–545.

[29] a T. Hirao, T. Moriuchi, T. Ishikawa, K. Nishimura, S. Mikami, Y. Ohshiro, I. Ikeda, A novel catalytic system for oxygenation with molecular oxygen induced by transition metal complexes with a multidentate *N*-heterocyclic podand ligand, J. Mol. Cata. A: Chem. 113 (1996) 117–130;
b A. Mishra, A. Ali, S. Upreti, R. Gupta, Cobalt coordination induced functionalized molecular clefts: isolation of $\{Co^{III}\text{-}Zn^{II}\}$ heterometallic complexes and their applications in beckmann rearrangement reactions, Inorg. Chem. 47 (2008) 154–161;
c A.P. Singh, R. Gupta, Copper(I) in the cleft: syntheses, structures and catalytic properties of $\{Cu^{+}\text{-}Co^{3+}\text{-}Cu^{+}\}$ and $\{Cu^{+}\text{-}Fe^{3+}\text{-}Cu^{+}\}$ heterobimetallic complexes, Eur. J. Inorg. Chem. 2010 (2010) 4546–4554;
d S. Srivastava, A. Ali, A. Tyagi, R. Gupta, $\{Cu^{2+}\text{-}Co^{3+}\text{-}Cu^{2+}\}$ and $\{Cu^{2+}\text{-}Fe^{3+}\text{-}Cu^{2+}\}$ heterobimetallic complexes and their catalytic properties, Eur. J. Inorg. Chem. 2014 (2014) 2113–2123;
e P. Pirovano, A.M. Magherusan, C. McGlynn, A. Ure, A. Lynes, A.R. McDonald, Nucleophilic reactivity of a copper(II)-superoxide complex, Angew. Chem. Int. Ed. 126 (2014) 6056–6060;
f M.K. Coggins, M.-T. Zhang, Z. Chen, N. Song, T.J. Meyer, Single-site copper(II) water oxidation electrocatalysis: rate enhancements with HPO_4^{2-} as a proton acceptor at pH 8, Angew. Chem. Int. Ed. 53 (2014) 12226–12230.

[30] D. Bansal, G. Kumar, G. Hundal, R. Gupta, Mononuclear complexes of amide-based ligands containing appended functional groups: role of secondary coordination spheres on catalysis, Dalton Trans. 43 (2014) 14865–14875.

[31] R. Kumar, N. Kaur, R. Kaur, N. Kaur, S.C. Sahoo, P.K. Nanda, Temperature controlled synthesis and transformation of dinuclear to hexanuclear zinc complexes of a benzothiazole based ligand: coordination induced fluorescence enhancement and quenching, J. Mol. Struct. 265 (2022) 133300.

[32] D. Bansal, S. Yadav, R. Gupta, Oxo-bridged tri- and tetra-nuclear cobalt complexes supported with amide-based nitrogen donor ligands, Eur. J. Inorg. Chem. 26 (2023) e202200601.

[33] K.M. Das, A. Thakur, Oxidative cross dehydrogenative coupling directed carbamates synthesis using cu(II) pincer complex as active catalyst under mild reaction condition, J. Heterocyclic Chem. **60** (***202***3) 1165–1178.

[34] E. Keskin, U. Solmaz, H. Arslan, NNN type pincer Pd (II) complexes of pyridine-2,6-dicarboxamides: catalytic activity and supramolecular formation, J. Mol. Struct. 1322 (2025) 140462.

[35] J.L. Bricks, G. Reck, K. Rurack, B. Schulz, M. Spieles, Cation coordination of bisamidopyridine-derived receptors as investigated in the solid-state and in solution, Supramol. Chem. 15 (2003) 189–197.

[36] G.C. Liu, H.X. Yu, H.Y. Lin, X.L. Wang, X.W. Li, Spacers-induced structural diversity of cobalt coordination polymers based on "V"-type dipyridylamide and dicarboxylic ligands: fluorescent, magnetic and photocatalytic properties, Polyhedron 126 (2017) 205–213.

[37] P. Kumar, S. Kaur, R. Gupta, K. Bowman-James, Pincers Based on Dicarboxamide and Dithiocarboxamide Functional Groups, in: D. Morales-Morales (Ed.), Pincer Compounds: Chemistry and Applications, Elsevier, 2018, pp. 295–325.

[38] S. Naskar, B. Jana, P. Ghosh, Anion-dependent thermo-responsive supramolecular superstructures of cu(II) macrocycles, Dalton Trans. 47 (2018) 5734–5742.

[39] C.E. Elwell, B.D. Neisen, W.B. Tolman, Copper complexes of multidentate carboxamide ligands, Inorg. Chim. Acta 485 (2019) 131–139.

[40] S. Abdolmaleki, M. Ghadermazi, F. Bagheri, H.A. Rudbari, G. Bruno, Evaluation of two novel macrocycles containing pyridine-2,6-dicarboxamide unit as cationic fluorescent sensor, Polyhedron 176 (2020) 114292.

[41] H. Rahimi, R. Hosseinzadeh, M. Tajbakhsh, A new and efficient pyridine-2,6-dicarboxamide-based fluorescent and colorimetric chemosensor for sensitive and selective recognition of Pb^{2+} and Cu^{2+}, J. Photochem. Photobiol. A Chem. 407 (2021) 113049.

[42] V. Kumar, P. Kumar, R. Gupta, Detection of Al^{3+} and Fe^{3+} ions by nitrobenzoxadiazole bearing pyridine-2,6-dicarboxamide based chemosensors: effect of solvents on detection, New J. Chem. 44 (2020) 13285–13294.

[43] D. Prabha, D. Singh, P. Kumar, R. Gupta, Selective detection of picric acid and pyrosulfate ion by nickel complexes offering a hydrogen-bonding-based cavity, Inorg. Chem. 60 (2021) 17889–17899.

[44] D. Prabha, D. Singh, R. Gupta, Selective turn-on sensing of fluoroquinolone drugs by zinc complexes of amide-based ligands, J. Chem. Sci. 133 (2021) 88, https://doi.org/10.1007/s12039-021-01956-9.

[45] P. Devi, S.M. Barry, K.M. Houlihan, M.J. Murphy, P. Turner, P. Jensen, P. J. Rutledge, Synthesis and structural characterisation of amides from picolinic acid and pyridine-2,6-dicarboxylic acid, Sci. Rep. 5 (2015) 9950, https://doi.org/10.1038/srep09950.

[46] E. Cadoni, P.R. Magalhães, R.M. Emídio, E. Mendes, J. Vítor, J. Carvalho, C. Cruz, B.L. Victor, A. Paulo, New (iso)quinolinyl-pyridine-2,6-dicarboxamide G-quadruplex stabilizers. A structure-activity relationship study, Pharmaceuticals 14 (2021) 669, https://doi.org/10.3390/ph14070669.

[47] R. Diószegi, D. Bonczidai-Kelemen, A.C. Bényei, N.V. May, I. Fábián, N. Lihi, Copper(II) complexes of pyridine-2,6-dicarboxamide ligands with high SOD activity, Inorg. Chem. 61 (2022) 2319–2332.

[48] K. Chaudhary, B. Agrahari, B. Biswas, N. Chatterjee, A. Chaudhary, A. Kumar, H. Sonker, S. Dewan, D. Saxena, A. Akhir, N. Malhotra, S. Chopra, S. Misra, S. Matheswaran, R.G. Singh, Pyridine-2,6-dicarboxamide proligands and their cu (II)/Zn(II) complexes targeting staphylococcus aureus for the attenuation of in vivo dental biofilm, Adv. Healthc. Mater. 13 (2024) e2400378, https://doi.org/10.1002/adhm.202400378. Epub 2024 Apr 23. PMID: 38621382.

[49] H.-Q. Tian, T. Jiang, H.-L. Shen, C. Huang, B.-X. Zhu, 1D coordination polymers constructed from pyridine-2,6-dicarboxamide ligands showing selective and recyclable adsorption toward methanol vapor, Cryst. Growth Des. 24 (2024) 1084–1095.

[50] T.S. Basu Baul, A. Khatiwara, M.R. Addepalli, B. Hlychho, A. Duthie, H. Gildenast, U. Englert, A.G. Mahmoud, M. Fatima C., Guedes da Silva, synthesis and structural characterization of diorganotin(IV) complexes with a tridentate N-heterocyclic podand ligand and investigation of their catalytic activity in Baeyer-Villiger oxidation of cyclic ketones to lactones, Appl. Organomet. Chem. 37 (**2023**) e7278.

[51] T.S. Basu Baul, S. Brahma, R. Tamang, A. Duthie, B. Koch, S. Parkin, Synthesis, structures, and cytotoxicity insights of organotin(IV) complexes with thiazole-appended pincer ligand, J. Inorg. Biochem. 262 (2025) 112750.

[52] K. Sisido, T. Takeda, J. Kinigawa, Direct synthesis of organotin compounds. I. Di- and tribenzyltin chlorides, J. Am. Chem. Soc. 83 (1961) 538–541.

[53] A. Meriem, M. Gielen, R. Willem, Synthesis, characterization and antitumour activity of a series of diorganotin(IV) derivatives of bis(carboxymethyl)amines, J. Organomet. Chem. 365 (1989) 91–101.
[54] A.M. Brouwer, Standards for photoluminescence quantum yield measurements in solution (IUPAC technical report), Pure Appl. Chem. 83 (2011) 2213–2228.
[55] R. Kumar, S.C. Sahoo, P.K. Nanda, A μ_4-Oxo bridged tetranuclear zinc complex as an efficient multitask catalyst for CO_2 conversion, Eur. J. Inorg. Chem. 2021 (2021) 1057–1064.
[56] S. Parkin, H. Hope, Macromolecular cryocrystallography: cooling, mounting, storage and transportation of crystals, J. Appl. Crystallogr. 31 (1998) 945–953.
[57] Bruker Programs APEX3, Smart, Saint. Bruker AXS Inc., Madison, Wisconsin, USA, 2016.
[58] L. Krause, R. Herbst-Irmer, G.M. Sheldrick, D. Stalke, Comparison of silver and molybdenum microfocus X-ray sources for single-crystal structure determination, J. Appl. Crystallogr. 48 (2015) 3–10.
[59] S. Parkin, B. Moezzi, H. Hope, XABS2: an empirical absorption correction program, J. Appl. Crystallogr. 28 (1995) 53–56.
[60] G.M. Sheldrick, G.M., SHELXT – integrated space-group and crystal-structure determination, Acta Crystallogr. A71 (2015) 3–8.
[61] G.M. Sheldrick, Crystal structure refinement with SHELXL, Acta Crystallogr. C71 (2015) 3–8.
[62] A.L. Spek, *PLATON SQUEEZE*: a tool for the calculation of the disordered solvent contribution to the calculated structure factors, Acta Crystallogr. C71 (2015) 9–18.
[63] D. Bansal, G. Hundal, R. Gupta, A metalloligand appended with thiazole rings: heterometallic {Co^{3+}-Zn^{2+}} and {Co^{3+}-Cd^{2+}} complexes and their heterogeneous catalytic applications, Eur. J. Inorg. Chem. 6 (2015) 1022–1032.
[64] D. Bansal, R., Gupta Chemosensors containing appended benzothiazole group(s): selective binding of Cu^{2+} and Zn^{2+} ions by two related receptors, Dalton Trans. 45 (2016) 502–507.
[65] C.F. Macrae, I. Sovago, S.J. Cottrell, P.T.A. Galek, P. McCabe, E. Pidcock, M. Platings, G.P. Shields, J.S. Stevens, M. Towler, P.A.J. Wood, Mercury 4.0: from visualization analysis, design and prediction, J. Appl. Crystallogr. 53 (2020) 226–235.